

# FIELD-ALIGNED AND GYRATING ION BEAMS IN THE EARTH'S FORESHOCK

C. Mazelle<sup>(1)</sup>, K. Meziane<sup>(2)</sup>, M. Wilber<sup>(3)</sup>

<sup>(1)</sup> Centre d'Etudes Spatiales des Rayonnements, CNRS, 9 Avenue du Colonel Roche, Toulouse, 31400, France (*Email: christian.mazelle@cesr.fr*)

<sup>(2)</sup> Physics Department, University of New Brunswick, Fredericton, NB, Canada

<sup>(3)</sup> Space Sciences Laboratory, University of California, Berkeley, USA

## ABSTRACT

The foreshock region is the first signature of the interaction of the solar wind with a planet's plasma environment when approaching its collisionless bow shock. Part of its structure and dynamic is determined by instabilities, which are created by the interaction of the solar wind with backstreaming ion populations. Large amplitude quasi-monochromatic low-frequency waves are often observed in the Earth's foreshock. Associated backstreaming ion distributions often reveal the existence of gyrating ions with well-defined pitch-angle and gyrophase organization around the local magnetic field. Field-aligned ion beams observed in the region close to the gyrating ions region are shown to be good candidate to generate the waves via the resonant ion/ion right-hand mode instability. The cyclotron resonance is quantitatively demonstrated for the first time from multi-spacecraft analysis by Cluster. Different mechanisms have been put forward to explain the existence of the gyrophase-bunched ions. The possibility of local nonlinear wave-particle interaction involving initially field-aligned beam ions is quantitatively shown by the good agreement between observed pitch-angles and those predicted from analytical test particle calculations.

## 1. INTRODUCTION

Several types of ion populations have been observed upstream of the Earth's bow shock and these population have been extensively studied and hypotheses have been put forward to explain their origin (*e.g.*, [1], and references therein). Ions beams of several keV collimated along interplanetary field lines have been observed upstream from the quasi-perpendicular shock. Downstream of the field-aligned beam region, distributions characterized by a gyromotion around the magnetic field, *i.e.* a non-vanishing perpendicular bulk velocity with respect to the background magnetic field, have been reported. These gyrating ion distributions are nongyrotropic or nearly-gyrotropic. Numerous studies concerning gyrating ions have been reported in earlier investigations mainly from ISEE 1 and 2 [2,3,4,5,6,7], AMPTE [8] and WIND [9,10]. Gyrating ions are often observed in association with ULF waves having

substantial amplitude [7]. The waves are right-handed and propagate nearly along the ambient magnetic field [*e.g.*, 4]. It is believed that the ULF waves are excited through a beam plasma instability resulting from the propagation of field-aligned ions which precede them closer to the foreshock boundary [11]. The produced waves can in turn trap the ions and cause the phase bunching of the distribution in what is called a beam disruption mechanism [12].

## 2. PREVIOUS OBSERVATIONS

*Fuselier et al.* [6] made a quantitative analysis of particle and monochromatic waves from ISEE data which strongly suggested that there was a coherent wave-particle interaction. They obtained a phase relationship between the gyrovelocity  $\mathbf{v}_\perp$  and the transverse wave field  $\delta\mathbf{B}_\perp$  so that energy transfer occurred between the particles and the waves and gyrophase trapping by the wave was possible. Since the field-aligned beams propagate deeply in the foreshock, the local production of gyrating ions through this process should be observed very far from the shock contrary to directly shock-produced gyrating ions which are subject to rapid gyrophase-mixing [13]. *Meziane et al.* [9] reported the first observations from WIND data of several gyrating ion distributions and their association with low frequency waves, at distances larger than  $20 R_E$  from the shock. There was again a clear indication of coherent wave-particle interaction. A more detailed study of the three-dimensional ion distributions with a large data set and the highest available time resolution (3s) has shown that these observational features can be found up to more than  $80 R_E$  from the shock [10]. Investigation of the non-linear wave trapping mechanism has shown that it can explain the properties of such gyrating ion distributions registered at large distances from the shock [14]. It has been shown that the particle are not only bunched in gyrophase but also trapped in pitch-angle in velocity space around a value which is directly related to the amplitude of the wave self-consistently generated by the original field-aligned ion beam.

### 3. CLUSTER OBSERVATIONS

*Mazelle et al.* [15] have investigated this local production mechanism to explain the existence of well-defined gyrating ion distributions reported from the Cluster CIS measurements in the Earth's foreshock. One example of such distributions is displayed on Fig. 1. For this event, Cluster s/c 3 was connected to the bow shock, during a much larger interval. At 2334:30 UT, energetic ions are revealed in the measurements by the high geometrical factor side of the HIA instrument. High fluxes are then continuously observed until 2344 UT. These ions are mostly propagating sunward, as revealed from the analysis of their guiding center velocity, i.e. they are backstreaming ions. Before 2334:30 UT, the interplanetary magnetic field (IMF) was nearly quasi-steady. Contrarily, prominent large amplitude low frequency waves are observed after 2335:45 UT both on the magnetic field and on the solar wind velocity. Fig. 1 displays three-dimensional 4-s representation of the ion distribution functions registered by CIS-CODIF. Nine consecutive distributions are shown for one energy channel ( $\sim 8$  keV) for which the observed backstreaming fluxes are maximum for this time interval. Each frame in Fig. 1 is a projection in gyrophase and pitch-angle with the  $\mathbf{B}$ -direction located at the center.

The three first snapshots indicate an ion beam propagating along the  $+\mathbf{B}$  direction with a parallel velocity of  $\sim 1,100$  km/s but the third one also shows a second peak for a large pitch-angle of about  $60^\circ$ . Then after 2335:45, the spacecraft has entered a gyrating ion region. Gyrating ions are identified by their gyrophase-restricted distribution peaked off the magnetic field direction. The interplanetary magnetic field used to plot the distributions is averaged over the spin interval (4 seconds) while the local proton cyclotron period is 7 seconds (i.e., about two ion sampling intervals). The gyrating distributions show a clear rotation of their maximum phase density in the left-handed sense around the magnetic field with alternating values separated by about  $180^\circ$ . Such gyrating ion distributions are observed up to  $\sim 2344$  UT.

Fig. 2 show an example of observations made by Cluster s/c 1 on 27 January 2003 for an interval in the ion Foreshock at a radial distance of  $18.8 R_E$ . The five first panels show energy-time spectrograms of ions from CIS/HIA respectively for solar wind sector and low sensitivity side (upper panel) showing the solar wind for reference and four solid angles ( $1\pi$  coverage around the  $+\mathbf{XGSE}$ ,  $-\mathbf{YGSE}$ ,  $+\mathbf{YGSE}$ , and  $-\mathbf{XGSE}$  looking directions respectively) from the high sensitivity side showing energetic foreshock ions. The four subsequent panels show interplanetary magnetic field components in GSE coordinates and its magnitude, respectively, from the FGM experiment (4-s averaged data). The three last panels respectively display the density and the

solar wind bulk velocity in GSE coordinates derived by moment calculations from HIA measurements (low sensitivity side).

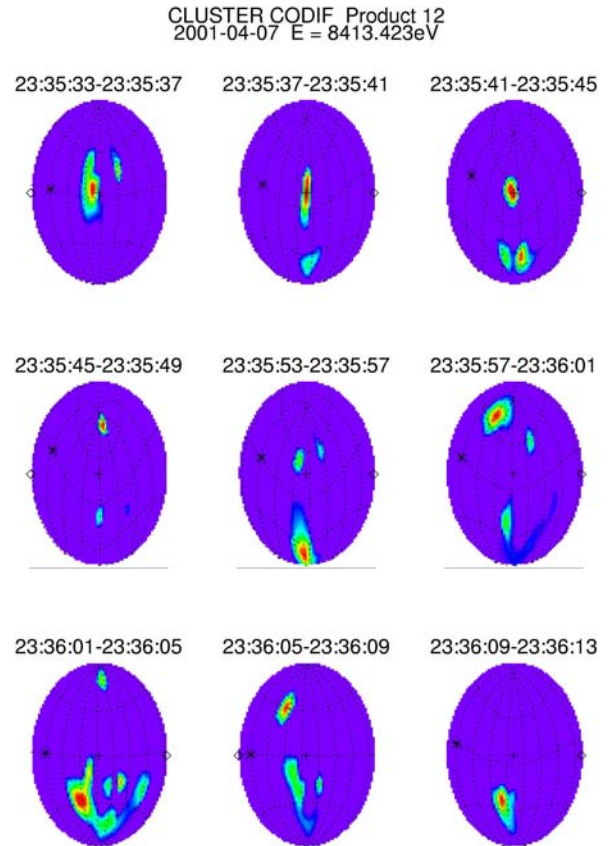


Fig. 1. Sequence of consecutive three-dimensional 4-s display of the proton angular distributions registered by CIS-CODIF for an energy of  $\sim 8$  keV (flux maximum). Each frame represents the normalized distribution function on a surface of constant energy in the solar wind frame of reference projected to display  $4\pi$ -coverage. The  $\mathbf{B}_0$  vector is located at the center of each plot (background field shown by a '+' identical for all frames) and the '\*' sign indicates the solar wind direction. For each frame, the maximum value of the normalized phase space density is shown in red (from [15]).

Again, Cluster s/c 1 was connected to the bow shock, during a much larger interval. From the beginning, energetic foreshock ions are revealed in the fifth energy spectrogram corresponding to the anti-sunward looking direction. These are backstreaming and field-aligned beams, since the  $B_x$  component is the main field component. The difference with the first panel showing the solar wind population is quite obvious. High fluxes are then continuously observed from 1849:30 UT in this sector while significant fluxes appear in the other sectors. Before this time, the IMF was quasi-steady.

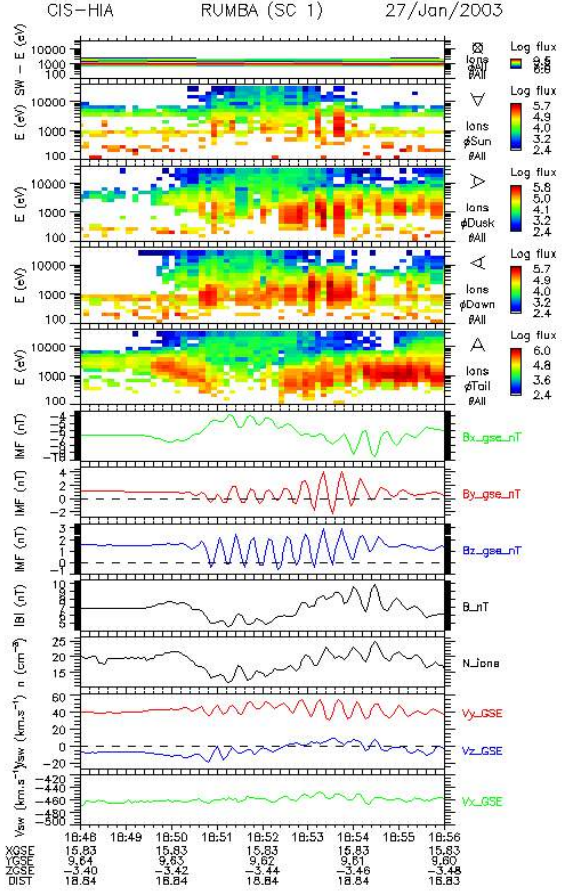


Fig. 2. Observations from CLUSTER CIS and FGM for an interval upstream from the Earth's bow shock : energy-time spectrograms of ions from CIS/HIA for solar wind ions (sunward looking direction and low sensitivity side - upper panel) and four solid angles for energetic foreshock ions (high sensitivity side), respectively; dc magnetic field components in GSE coordinates and its magnitude; solar wind ion density and bulk velocity in GSE coordinates.

Contrarily, prominent quasi-sinusoidal large amplitude low frequency waves are observed after  $\sim 1850$  UT. Then the wave amplitude remains large until  $\sim 1856$  UT particularly on the  $B_y$  and  $B_z$  components (with a peak-to-peak amplitude up to about 6 nT around 1855:30 UT) revealing their mainly transverse nature. The waves are also observed on the solar wind velocity, mainly on the  $V_y$  and  $V_z$  components (peak-to-peak amplitude up to 35 km/s) as well as on the proton density in correlation with the magnetic field magnitude, which shows the waves also possess a little compressive nature. After 1850:36 UT, the 3-D ion distributions reveal gyrating ions as on Fig. 1. For the former case, large amplitude low frequency waves appear on the dc magnetic field components appear after 2335:45 UT, the very time when the energetic backstreaming ion distributions on Fig. 1 change from field aligned beam-like to gyrophase bunched shape [15]. These observational features such as the alternation between field-aligned beams without

waves and gyrating ions with quasi-monochromatic large-amplitude waves are typical for all the gyrating ion events discussed here.

## 4. WAVE PROPERTIES AND EXCITATION

### 4.1. Analysis of the low frequency waves

The large amplitude low frequency waves associated with the gyrating ions have been systematically analyzed using multi-spacecraft analysis techniques [e.g., 16] applied to the magnetic field data [17, 18, 19] as was done for one case-study in [15]. We have first studied the magnetic fluctuations observed on each of the 4 spacecraft by using the classical minimum variance analysis (MVA) technique (see e.g. [20] and references therein). This characterizes the waves, giving the direction of propagation with respect to the background magnetic field  $\mathbf{B}_0$ , the polarization and the relative wave amplitude  $\delta B/B_0$ . The usual convention is used to order the eigenvalues of the covariance matrix of the field perturbations  $\lambda_1 > \lambda_2 > \lambda_3$  (maximum, intermediate and minimum variances, respectively). The direction of minimum variance gives the direction of propagation with respect to the background magnetic field  $\mathbf{B}_0$ , computed as the averaged field vector during the time interval analyzed, and provides the angle  $\theta_{\mathbf{k}B}$  between the wave vector  $\mathbf{k}$  and  $\pm \mathbf{B}_0$ . The quality of this determination is measured via the value of the eigenvalue ratio  $\lambda_2/\lambda_3$ . This one must be at least equal to 3 to give reliable results whereas a value larger than 10 is usually more suitable. Fig. 3 illustrates an example of these results obtained for one satellite. The observed period in the spacecraft frame, computed from the mean interval between magnetic field wave crests for all components, is  $23 \pm 2$  s while the local proton gyroperiod is about 7 s.

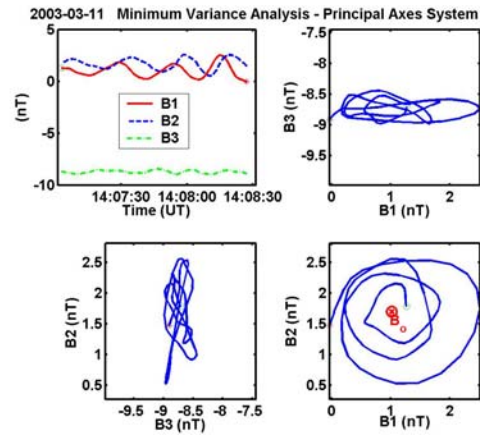


Fig. 3. Example of results from the minimum variance analysis of the magnetic field waves associated with gyrating ions in the Earth's foreshock.

The upper left panel shows the time sequences of the magnetic field components in the principal axes coordinate system and the other panels the corresponding hodograms. The waveform is regular and quasi-monochromatic and the hodograms reveal that the wave field vector remains in a well-defined plane with a very accurate determination of its normal vector ( $\lambda_2/\lambda_3=40.1$ ). The minimum variance direction provides a direction of propagation nearly parallel to the ambient magnetic field  $\mathbf{B}_0$ , computed as the averaged field for the time interval studied ( $\theta_{kB}=12\pm 2^\circ$ ). The waves are nearly circularly ( $\lambda_1/\lambda_2=1.3$ ) and left-hand polarized with respect to  $\mathbf{B}_0$  in the spacecraft frame, as shown on the hodogram in the principal variance plane, with an observed period (Doppler-shifted) much larger than the local proton gyroperiod. The wave is mainly transverse ( $|\delta B_\perp|/B_0=0.2$ ) but the compressive component is not negligible with  $|\delta B_\parallel|/B_0 \approx \delta|B_0|/B_0=0.05$  comparable with the relative proton density variation. The low frequency waves observed on the interplanetary magnetic field on the three other satellites are very similar and consequently the results obtained by the MVA technique are very similar. The multi-spacecraft timing analysis techniques provide a very similar wave vector direction but without ambiguity relative to the sense. Moreover it gives both the value of the wave phase velocity and the rest frame frequency [17, 18].

These foreshock LF waves associated with the gyrating ions have very common properties compared to previous observations (e.g. [6]): they are mainly transverse, propagating close to the background field (with a small obliquity) with a phase velocity close to the Alfvén speed  $V_A$  and co-streaming with the foreshock backstreaming particles, *i.e.*, mainly against the solar wind flow [so that they are subject to anomalous Doppler shift and polarization reversal from the plasma frame to the s/c frame implying that they are intrinsically right-hand mode waves] with a frequency in the plasma frame that is typically  $\Omega_p/10$ , where  $\Omega_p$  is the proton gyrofrequency, and a wavelength of the order of one Earth's radius. These right-hand mode waves are called '30-s waves'. Their amplitude can be very large ( $|\delta \mathbf{B}|/B_0 \approx 1$ ).

## 4.2. Cyclotron resonance

While it was expected that the '30-s waves' are generated by a resonant ion/ion electromagnetic instability [11], this was never quantitatively demonstrated before Cluster since it was not possible from single or even dual-spacecraft measurements to derive unambiguously both the wave rest frame frequency and phase velocity without making any assumption. The cyclotron resonance condition with the right-hand mode writes:

$$\omega - k_\parallel V_{\parallel} + \Omega_p = 0 \quad (1)$$

where  $\omega$  is the wave frequency in the solar wind rest frame,  $k_\parallel$  is the component of the wave vector parallel to the background magnetic field, and  $V_{\parallel}$  is the parallel component of the resonant ion velocity (solar wind frame). In the spacecraft frame, these waves would have a Doppler-shifted frequency of

$$\omega' = \omega + \mathbf{k} \cdot \mathbf{V}_{sw} = \omega + k_\parallel V_{sw} \cos \theta_{kV} / \cos \theta_{kB} \quad (2)$$

where  $\theta_{kV}$  is the angle between the wave vector and the direction of the solar wind velocity  $\mathbf{V}_{sw}$ . Then using the experimental values, we have computed the predicted wave periods  $T_{pred} \equiv 2\pi/\omega'$  in the spacecraft frame according to (2) if there is cyclotron resonance by taking  $k_\parallel$  from (1) using the measured ion parallel velocity  $V_{\parallel}$  and compared  $T_{pred}$  with the observed period  $T_{obs}$ .

For all the gyrating ion distributions analyzed the associated predicted periods are systematically a little smaller but close to the observed value, taking into account the experimental uncertainties. The deduced parallel wavelengths  $\lambda_\parallel$  of these predicted resonant waves all are of the order of  $1 R_E$ , which is consistent with the above results. Moreover if one assumes exact local cyclotron resonance with the local waves solving the linear system made by (1) and (2) without any approximation, this always leads to wave properties different but very close to those previously deduced from the observations. This strongly supports the possibility that local wave-particle interaction occurs for these distributions. These waves propagating upstream in the solar wind frame at a phase speed much smaller than  $V_{sw}$  are simply blown back by the solar wind and interact with the local backstreaming distributions leaking upstream with a much larger parallel velocity ( $V_{\parallel} \sim 10 V_A$ , typically). Although the gyrophase-bunched ion distributions still contain a large amount of free energy to generate this kind of wave, this does not necessarily imply, however, that the waves are locally produced by the observed distributions. Moreover, a more careful analysis reveals that the observed parallel velocities of the local gyrating distributions appear generally a little bit too small for  $T_{pred}$  to match  $T_{obs}$ . As revealed in Fig. 1, field-aligned beams are clearly observed just before the gyrating distributions and their characteristics can be derived. We then make the same test of period matching for the field-aligned beams. To illustrate that, for the distribution dated from 2335:37 UT in Fig. 1,  $V_{\parallel} = 1060 \pm 50$  km/s which gives  $T_{pred} = 25.4$  s while  $T_{obs} = 25 \pm 2$  s. This shows that the field-aligned beam observed at the edge of the gyrating ion region is in exact cyclotron resonance with the wave observed with the gyrating ions. Thus, such a field-

aligned beam distribution could have generated the observed wave from the resonant right-hand ion/ion beam instability. We have applied the same test to some other events. These results are shown graphically on Fig. 4.

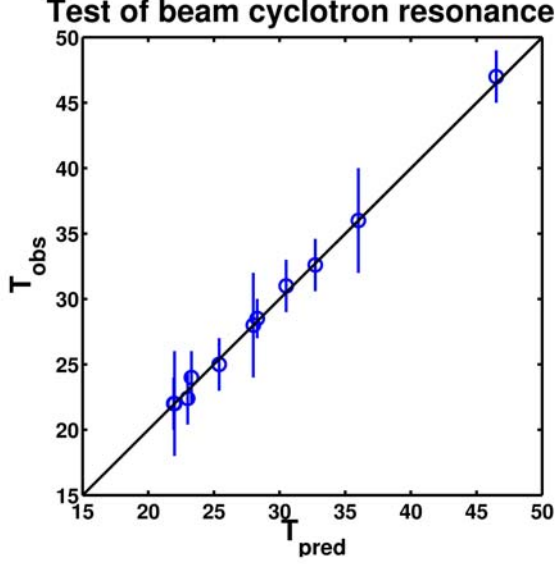


Fig. 4. Comparison between the observed periods and the predicted periods in the spacecraft frame when assuming cyclotron resonance with field-aligned beams observed at the edge of the gyrating ions/low frequency waves regions (11 different events).

The very good agreement between the observed and the predicted periods is the first direct quantitative evidence so far of this cyclotron resonance from observations in the ion foreshock.

### 4.3. Wave generation

To test the wave generation hypothesis, we solve the linear Maxwell-Vlasov dispersion relation for parallel electromagnetic modes. We use a plasma model with parameters from the CLUSTER observations. As expected only the ion/ion right-hand mode is found to be unstable for the local plasma parameters. The results are shown for one example already discussed in [15] on Fig. 5. The real frequency and the phase velocity at the growth rate maximum are in very good agreement with the value in the plasma frame computed from the observations ( $\sim V_A$ , typically). The associated parallel wavelength is  $\lambda_{max} = 6,670$  km, in very good agreement with the experimental value  $\lambda_{exp} = 7,000 \pm 300$  km  $\sim 1.05 R_E$  and also with the value deduced from the cyclotron resonance condition (1),  $\lambda_{max} = 6,700$  km. This helps to conclude that the observed field-aligned beam or at least a beam with similar properties (density, drift velocity and temperature) is a very good candidate to be the source of the waves observed with the gyrating ion distributions. We have performed the same linear

analysis for the other events of Fig. 4 and also got good agreement with the observed waves.

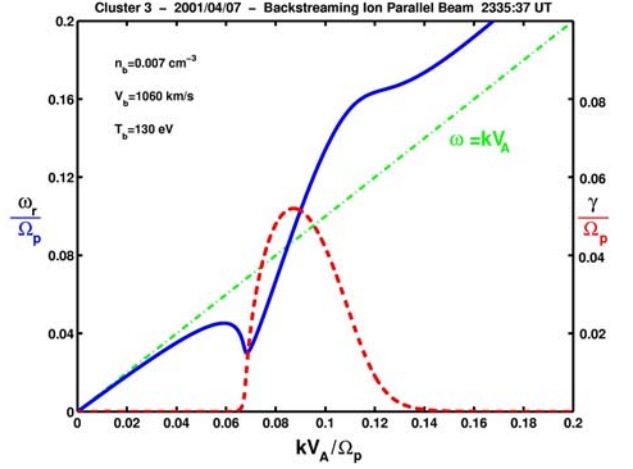


Fig. 5. Real frequency (solid line) and growth rate (dashed line) of the ion/ion right-hand resonant instability as functions of the normalized wavenumber at propagation parallel to  $\mathbf{B}_0$  for experimental parameters suitable for the field-aligned beam distribution shown on the second display of Fig. 1 (from [15]).

## 5. ORIGIN OF THE PHASE-BUNCHING

### 5.1. Nonlinear 'pitch-angle trapping'

The events reported here are inconsistent with a specular reflection at the Earth's bow shock. For instance, the observed pitch-angles of the gyrating ions on Fig. 1 are much too large (it should be nearly  $\theta Bn$ , e.g., [21], which here has been found to be close to  $30^\circ$ ). It is thus necessary to invoke a local production mechanism for these upstream distributions. For this, we make some theoretical considerations about the nonlinear trapping of ions by an electromagnetic monochromatic wave. From the equation of motion of a particle of velocity  $\mathbf{v}$  in the frame moving along the dc magnetic field  $\mathbf{B}_0$  ( $//z$ ) at the phase velocity  $V_\phi$  ( $\ll c$ ) of a monochromatic wave, propagating along  $\mathbf{B}_0$  with a constant amplitude  $B_1$ , it is easy to deduce two constants of the motion [e.g., 22, 23, 24]:

$$T = w_{//}^2 + w_{\perp}^2 = C_1 \quad (3)$$

$$\text{and } S = (w_{//} - 1)^2 - 2 \frac{\Omega_1}{\Omega_0} w_{\perp} \sin \psi = C_2 \quad (4)$$

$$\text{where } \mathbf{w} = \frac{k//}{\Omega_0} \mathbf{v}, \quad \Omega_{0,1} = \frac{qB_{0,1}}{m}, \quad \psi = \varphi + k//z$$

and  $\varphi$  is the gyrophase angle. The invariance of  $T$  is simply the conservation of total particle energy in the wave frame (no electric field in this frame). The

invariant  $S$  relates the parallel and perpendicular motion of the particles. Using the particle equations of motion with (3) and (4), it is possible to show that  $S$  can be used as a Hamiltonian of the particle motion and that the system is solvable by a quadrature

$$\frac{dw_{//}}{dt} = \pm \frac{\Omega_0}{2} \sqrt{4 \left( \frac{\Omega_1}{\Omega_0} \right)^2 \sin^2 \psi (C_1 - w_{//}^2) - [(w_{//} - 1)^2 - C_2]^2} \quad (5)$$

which can be solved in terms of elliptic integrals as for a pendulum equation. The particle is thus 'trapped' in velocity space like in a 'potential well'. Using the pitch-angle  $\alpha$  such as  $\tan \alpha = w_{\perp} / w_{//}$ , the equations of motions

$$\frac{d\alpha}{dt} = -\delta \cos \psi \quad (6)$$

and 
$$\frac{d\psi}{dt} = \delta \cot \alpha \sin \psi + \sqrt{T} \cos \alpha - 1 \quad (7)$$

where 
$$\delta = \frac{\Omega_1}{\Omega_0} = \frac{\delta B_{\perp}}{B_0} \quad (8)$$

can be derived from the Hamiltonian  $S(\alpha, \psi)$ . This Hamiltonian has a singularity for  $\psi = \pi/2$  which is the only one to be considered since the pitch angle  $\alpha$  is defined in the interval  $[0, \pi]$ . As a first step, we consider a mono-energetic parallel ion beam, i.e. this means from equations (3), (4) and (7) that we have  $T=1$ . Then, by linearizing the trapping potential, around  $\psi = \pi/2$ , it is straightforward to show that this singularity corresponds to a value  $\alpha_0$ , defining the center of the trapping cells which depends only on the value of  $\delta$  [for small values of  $\alpha_0$ , it is possible to use the approximation  $\alpha_0 \approx (2\delta)^{1/3}$ ]. If  $V_{//0}$  is the initial velocity of the cyclotron resonant beam (i.e.,  $T=1$ ), the nonlinear interaction will tend to create a peak in the distribution around the center of the trapping cell in phase space associated with the pitch angle  $\alpha_0$  in the 'wave frame'. The theoretical pitch-angle distribution in the plasma frame can be computed from the observed wave amplitude and wave phase velocity (Fig. 6).

## 5.2. Comparison with experimental results

We have used the experimental parallel and perpendicular velocities for the observed gyrating ion distributions corresponding to the time intervals where we have analyzed the low frequency waves to compute the associated pitch-angles in the wave frame (using the experimental wave phase speed). To illustrate this, for the event described in Fig. 1, the mean experimental pitch-angle is  $\alpha_{exp} = 60 \pm 5^\circ$  while the theoretical value is  $\alpha_{theory} = 59.8^\circ$  using the mean value  $\delta = 0.85$  from the observations [15]. But in order to better test the theory

it was necessary to accumulate more statistics. We have performed the same analysis for different events. For some of them, the amplitude clearly change for different time intervals so that we have considered them independently. This gives the opportunity to test the model for a large range of wave amplitude and pitch-angle. The comparison between  $\alpha_{exp}$  and  $\alpha_{theory}$  is displayed graphically on Fig. 7.

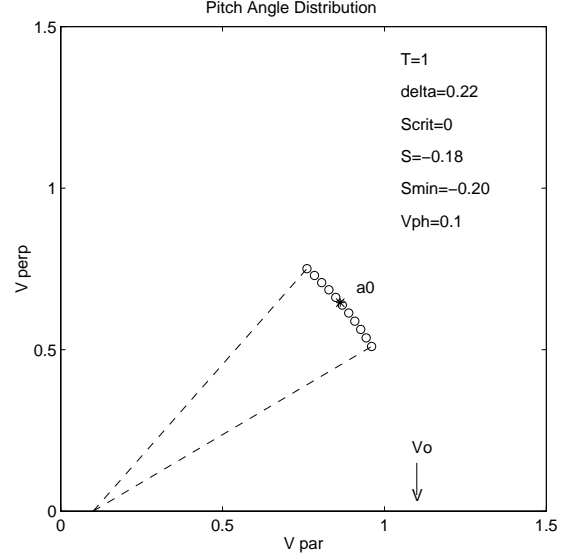


Fig. 6. Theoretical particle distribution in the  $(V_{//}, V_{\perp})$  plane displaying the pitch-angle width for a constant value of the second invariant of the movement  $S(\alpha, \psi)$ .  $V_0$  is the initial velocity of the cyclotron resonant beam from [14].

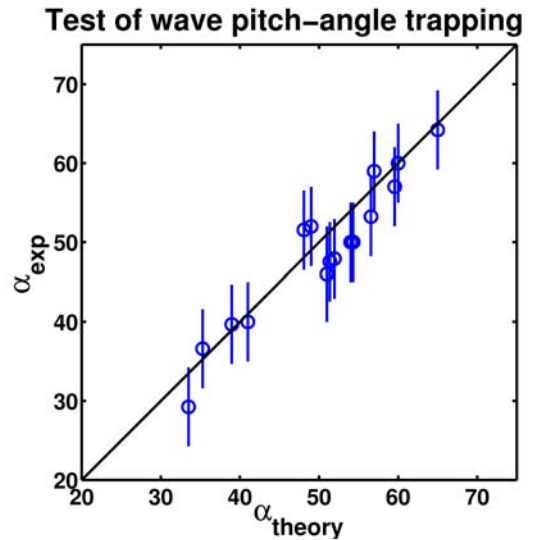


Fig. 7. Comparison between the mean experimental pitch-angle in the 'wave frame' and the theoretical value computed from the experimental wave amplitude.

The good agreement revealed in Fig. 7 strongly suggests the possible scenario that the quasi-monochromatic

waves generated from the ion/ion beam instability could then have non-linearly trapped the ions to produce the resulting gyrating distributions.

Finally we have checked the conservation of the total energy in the 'wave frame' which is one of the hypothesis of the theory. Note that is strictly valid only for a purely parallel propagating wave. The small obliquity of the observed waves implies a small parallel electric field which cannot be cancelled in the 'wave frame' as defined previously and thus a certain amount of acceleration/deceleration can be anticipated. We can first make this check for each individual event/interval by looking at the experimental peak pitch-angle distribution in the 'wave frame'. Fig.8 displays the results for the ion distributions shown on Fig.1 which are represented by the asterisks encircled by an ellipse (pitch-angles around  $60^\circ$ ). A straight line for the theoretical pitch-angle is also shown. The locus of the initial resonant field-aligned beam is shown by an asterisk on the  $V_{\parallel}$  axis. We have also drawn the representation in the  $(V_{\parallel}, V_{\perp})$  plane of the constant energy sphere in the 'wave frame' which contains the locus of the initial beam and a second one shifted by 50 km/s taking into account the experimental accuracy from the instrument. While the loci representing the gyrophase-bunched ions are closer to this second sphere which could be due to some acceleration, we can consider that the agreement with the simple assumption of energy conservation is quite good as a first approximation in the limit of the experimental capabilities.

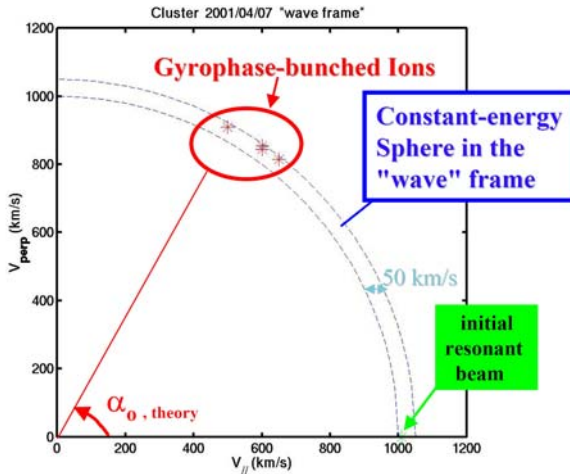


Fig. 8. Peak pitch-angle distributions in the 'wave frame' for the ion distributions shown on Fig. 1 .

We have then make the same test for the other events. Fig. 9 displays the comparison between the radius of each energy sphere with the associated field-aligned beam velocity in the 'wave frame'. Despite the quite large experimental error bars the agreement is generally quite good which also emphasizes the capability of the

simple theory used here to reproduce observations.

### Test of wave frame energy conservation

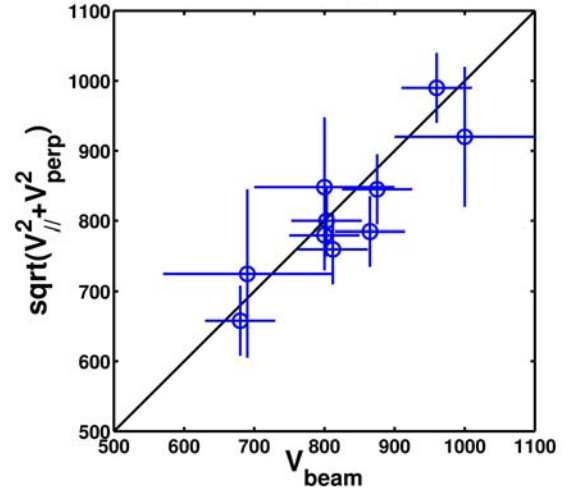


Fig.9. Comparison between the energy sphere radius for the gyrating ions compared to the associated field-aligned beam velocity in the 'wave frame' .

## 6. CONCLUSION

The possibility of producing the observed gyrophase-bunched ion distributions from the disruption of the beam by the excited wave has led to a good quantitative agreement from a nonlinear trapping theory which predicts that the pitch-angle of the final gyrating ion distribution is related to the wave amplitude [14]. This result is very similar to those obtained from previous studies in the distant foreshock (up to  $80 R_E$ ) from Wind data with lower backstreaming ion densities and wave amplitude [9, 10, 14], which could mean that the present study corresponds to the same mechanism observed by Cluster closer to the bow shock. Other gyrating ion events have been identified in the Cluster data [25]. We must notice that most of them appear consistent with this trapping mechanism while to date only one event with gyro-phased bunched ions consistent with a production by specular reflection at the bow shock surface has been identified [21]. The analytical test-particle calculations of the nonlinear interaction between a field-aligned beam and the single self-generated cyclotron-resonant wave briefly described here cannot tell anything about the physical description during the wave growth. Numerical simulations are necessary for that. Previous studies [e.g., 12] led to pitch-angle diffusion though the production mechanism of gyrophase-bunched ion distributions is a coherent process and not a diffusive one. It would be therefore strongly necessary to conduct new numerical kinetic simulations to better understand this pitch-angle trapping process and quantify the life-time of the gyrophase-bunched distribution in comparison with observations.

## REFERENCES

1. Fuselier, S. A., *Geophysical Monograph 81*, p107-119, 1994.
2. Eastman, T.E., R.R. Anderson, L.A. Frank, G.K. Parks, *J. Geophys. Res.*, 86, 4379-4395, 1981.
3. Gosling, J. T., M. F. Thomsen, S. J. Bame, W. C. Feldman, G. Paschmann, and N. Sckopke, *Geophys. Res. Lett.*, 87, 1333–, 1982.
4. Thomsen, M. F., J. T. Gosling, S. J. Bame, and C. T. Russell, *J. Geophys. Res.*, 90, 267, 1985.
5. Fuselier, S. A., M. F. Thomsen, J. T. Gosling, S. J. Bame, and C. T. Russell, *J. Geophys. Res.*, 91, 91–, 1986.
6. Fuselier, S. A., M. F. Thomsen, S. P. Gary, S. J. Bame, C. T. Russell, and G. K. Parks, *Geophys. Res. Lett.*, 13, 60–63, 1986.
7. Fuselier, S. A., J. T. Gosling, and M. F. Thomsen, *J. Geophys. Res.*, 91, 4163–4170, 1986.
8. Fazakerley, A.N., A.J. Coates, and M.W. Dunlop, *Adv Space Res*, 15, (8/9)103-106, 1995.
9. Meziane, K., *et al.*, *Adv. Space Res.*, 20, n°4, pp. 703-706, 1997.
10. Meziane, K., C. Mazelle, R. P. Lin, D. LeQuéau, D. E. Larson, G. K. Parks, and R. P. Lepping, *J. Geophys. Res.*, 106, 5731–5742, 2001.
11. Gary, S. P., J. T. Gosling, and D. W. Forslund, *J. Geophys. Res.*, 86, 6691–, 1981.
12. Hoshino, M., and T. Terasawa, *J. Geophys. Res.*, 90, 573–, 1985.
13. Gurgiolo, C., G. K. Parks, and B. H. Mauk, *J. Geophys. Res.*, 88, 9093–, 1983.
14. Mazelle, C., D. Le Quéau, and K. Meziane, *Nonlinear Processes in Geophysics*, 7, 185-190, 2000.
15. Mazelle, C., K. Meziane, D. Le Quéau, M. Wilber, J.P. Eastwood, *et al.*, *Planet. Sp. Science*, doi:10.11016/j.pss.2003.05.0, 51, 785-795, 2003.
16. Schwartz, S. J., Shock and discontinuity normals, Mach numbers, and related parameters, in *Analysis Methods for Multi-spacecraft Data*, G. Paschmann and W. Daly (Eds.), *ISSI Scientific Report*, 1998.
17. Eastwood, J.P., A. Balogh, M.W. Dunlop, T.S. Horbury, I. Dandouras, *Geophys. Res. Lett.*, 29, No. 22, 2046, doi:10.1029/2002GL015582, 2002.
18. Eastwood, J.P., A. Balogh, E. Lucek, C. Mazelle, and I. Dandouras, *Annales Geophysicae*, 21, 1457-1465, 2003.
19. Eastwood, J.P., A. Balogh, C. Mazelle, I. Dandouras, and H. Rème, *Geophys. Res. Lett.*, 31(4), 4804, doi: 10.1029/2003GL018897, 2004.
20. Sonnerup, U.Ö , and M. Scheible, Minimum and Maximum Variance Analysis, in *Analysis Methods for Multi-spacecraft Data*, G. Paschmann and W. Daly (Eds.), *ISSI Scientific Report*, 1998.
21. Meziane, K., C. Mazelle, M. Wilber, D. Le Quéau, J.P. Eastwood, *et al.*, *Annales Geophys.* 22: 1–11, SRef-ID: 1432-0576/ag/2004-22-1, 2004.
22. Gendrin, R., *Astrophysics and Space Science*, 28, 245-266, 1974.
23. Matsumoto, H., *Space Science Reviews* 42, 429-448, 1985.
24. Le Quéau, D., and A. Roux, *Solar Physics* 111, 59-80, 1987.
25. Meziane, K., M. Wilber, C. Mazelle, D. Le Quéau, H. Kucharek, *et al.*, *J. Geophys. Res.*, 109, A05107, doi:10.1029/2003JA010374, 2004.